Preprints of the 21st IFAC World Congress (Virtual)
Berlin, Germany, July 12-17, 2020

Trajectory Tracking and Adjustable Stiffness Control of a Pneumatically Actuated Robot

Adrian Raisch * **Axel Thallemer** ** **Aleksandar Kostadinov** ***
Oliver Sawodny *

* *Institute for System Dynamics, University of Stuttgart, Germany (e-mail: {raisch, sawodny}@isys.uni-stuttgart.de).*
** *The Hong Kong University of Science and Technology / SENG School of Engineering / ISD Division of Integrative Systems & Design, Clear Water Bay, Kowloon, Hong Kong (e-mail: thallemer@ust.hk).*
*** *National University of Singapore / SDE School of Design and Environment / DID Division of Industrial Design (e-mail: kostadinov.aleksandar@u.nus.edu).*

Abstract: Variable stiffness actuation and soft robotics are growing fields of interest in research due to their close link to the feasibility of human-machine-interaction. In this paper, we give the modeling and control of a pneumatically actuated robot with three degrees of freedom based on the antagonist principle. The use of pneumatic actuators brings the benefit of an inherit softness and utilizing the mean force of the antagonists, we can influence the stiffness of the overall system. We present a cascaded control concept using feedback linearization for the pneumatics, decoupling the mechanical dynamics, and taking into account the constructive limitations to the available torque. The control concept is then applied to the robot in an experimental setup and its performance is validated.

Keywords: Pneumatic Servo Systems, Mechatronics, Pneumatic Muscle Actuator, Robotics, Feedback linearization.

1. INTRODUCTION

One of today's challenges in robotics and automation is the interaction of man and machine with its deriving requirements for safety and control concepts. As a human operator must not be harmed by a machine he is interacting with, special concepts for preventing and handling the contact of man and machine are necessary. From this standpoint the field of variable stiffness actuation and soft robotics arises, bringing a flexibility into robotics and therefore a certain safety level into the human-machine-interaction (Bicchi and Tonietti (2004)).

In literature, there exist different control concepts for soft robotics applications – an overview on such and their control techniques is given in Albu-Schäffer et al. (2008) and Verl et al. (2015). The commonly employed concept of variable stiffness actuation can be realized by two approaches in general: by design or by control of actuators (Vanderborght et al. (2013)). Examples for the practical application of variable stiffness by design can be found in Grebenstein et al. (2011) where a combination of electromechanical motors and a variable stiffness mechanism is used to give the robot its softness, in Laffranchi et al. (2013) where a variable damping mechanism is used to achieve a compliant behavior, or in Jafari et al. (2014) where an actuator with an adjustable stiffness is presented. On the other hand, the variable stiffness of the actuators can also be achieved by control: an example for this is found in Boaventura et al. (2012), where a variable impedance feedback control is applied to the hydraulic actuators. In Ficuciello et al. (2015) redundant manipulators are considered, and in Kronander and Billard (2016) the stability for robotic manipulators under variable impedance control is investigated.

In contrast to electromechanical or hydraulic drives as seen in the previous examples, the use of pneumatic actuators brings an inherent softness due to the compressibility of air. For the actuation of robots using pneumatics there exist different concepts for realization: in Taghia et al. (2012), a pneumatically actuated robot with rotary joints is presented. The Bionic-Handling-Assistant (Falkenhahn et al. (2017)) realizes a soft continuum-robot-approach. By using pneumatic artificial muscles, a large force to weight ratio is given due to their low mass. Examples for robots driven by such pneumatic artificial muscles are found in Ament and Eichhorn (2010), Hildebrandt et al. (2005), or Wang et al. (2013).

1.1 Main Contributions

In the present paper, we give the modeling and control of a novel robot with three rotational degrees of freedom actuated by pneumatic artificial muscles. The assembly of the robot reminds of the human arm. Figure 1 illustrates the experimental setup: the three rotary joints of the robot are actuated based on the antagonist principle.

Fig. 1. Experimental setup of the robot actuated by pairs of pneumatic muscles. The three rotary degrees of freedom will later be denoted by α_1, α_2, and α_3. In the experimental setup, the three angles, as well as the pressures of the pneumatic muscles, pneumatic valves, and of the air supply are measured in order to apply the feedback controller.

Once a pneumatic muscle is put under pressure, it causes a traction force and contracts. Utilizing their lever, the antagonists of each joint produce a resulting momentum and thus put the robot into motion. In this paper, we present a cascaded control scheme for the robot. In an inner control loop, the pressure of the eight pneumatic muscles is controlled via exact feed-back linearization. An outer control loop adds a angle control based on a computed torque ansatz decoupling the system and allowing to apply linear control techniques. Via the mean force of the pneumatic muscles acting on a joint, we can then specify the stiffness of the overall system.

1.2 Outline of the Paper

The remainder of this paper is organized as follows: After this brief introduction, we give the modeling of the system in Section 2 and present the control design in Section 3. In Section 4, we show our experimental results and end up with a short conclusion in Section 5.

2. MODELING

This section presents the mathematical model of the robot. To distinct its eight pneumatic muscles we use the index

$$i \in \{1, \dots, 8\}$$

throughout the paper. From a mechanical point of view, the robot has three rotary joints which we will address by the index

$$l \in \{1, 2, 3\}.$$

In our setup, each of the three joints is actuated by at least one pair of muscles (compare Figure 1):

- The first joint α_1 is actuated by a pair of Festo DMSP-20 muscles ($i = 1, 2$),
- The second joint α_2 is actuated by two pairs of Festo DMSP-10 muscles ($i = 3, \dots, 6$),
- The third joint α_3 is actuated by one pair of Festo DMSP-10 muscles ($i = 7, 8$).

With this configuration, the joints can be actuated with a decreasing torque in their serial order – similar to the expected torque requirements of the joints.

2.1 Pneumatic Model

The robot is actuated by eight pneumatic muscles. The behavior of pneumatic muscles with respect to force and volume has been investigated in Chou and Hannaford (1996). For a simplified model, the muscle forces F_i and volumes V_i are approximated by polynomial functions (Hildebrandt et al. (2003))

$$F_i(p_i, s_i) = (p_i - p_0) \sum_{k=0}^{5} b_k s_i^k, \qquad i = 1 \dots 8 \tag{1}$$

$$V_i(s_i) = \sum_{k=0}^{3} c_k s_i^k, \qquad i = 1 \dots 8 \tag{2}$$

in dependance of their pressure p_i and contraction s_i, and the ambiance pressure p_0. The relation approximated by (1) is a monotonically increasing function of pressure and muscle length: the more a muscle is stretched or put under pressure, the higher its traction force becomes. The volume function (2) reveals to be independent of pressure, but decreasing with the muscle's length: an inflated muscle has a larger volume and shorter length than a deflated muscle.

The air inside the muscle is assumed to behave as an ideal gas, i.e. the ideal gas law

$$p_i V_i = m_i R_s T \tag{3}$$

applies. Here, m_i represents the mass of air inside the muscle, R_s is the specific gas constant of dry air, and T is the temperature which we assume to be constant.

Furthermore, the surface of the muscle allows a partial heat flow to the ambiance. Therefore, a change of pressure or volume inside the muscle can be described by a polytropic process with

$$p_i V_i^{\kappa} = \text{const.} \tag{4}$$

The total differential of (3) combined with (4) results in the pressure dynamics

$$\dot{p}_i = \frac{\kappa}{V_i(s_i)} \left(R_s T \dot{m}_i - p_i \dot{V}_i(s_i, \dot{s}_i) \right). \tag{5}$$

The mass flow $\dot{m}_i$ in (5) is a result of the pressure difference at the valve. The valves used in our experimental setup are 3/3 proportional valves and as supply pressure we use 8bar. With the density of air ρ, the conductance C depending on the control signal v, and pressures $p_i^{\text{prim}} \geq p_i^{\text{sec}}$, the mass flow into the muscle can be expressed by

$$\dot{m}_i = \rho\, p_i^{\text{prim}} C(v) \Psi \left(\frac{p_i^{\text{sec}}}{p_i^{\text{prim}}}, b \right). \tag{6}$$

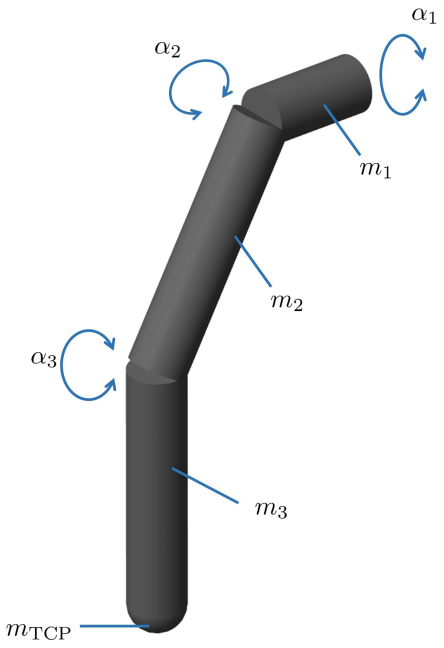

Fig. 2. Sketch of the mechanical multibody system: It contains three cylindrical bodies connected by revolute joints.

The flow function Ψ of the valve is depending on the ratio of upstream (primary) and downstream (secondary) pressure, i.e. the pressure in front of and behind the valve:

$$\Psi\left(\frac{p_i^{\mathrm{sec}}}{p_i^{\mathrm{prim}}}, b\right) = \begin{cases} \sqrt{1 - \left(\frac{\frac{p_i^{\mathrm{sec}}}{p_i^{\mathrm{prim}}} - b}{1-b}\right)^2} & \frac{p_i^{\mathrm{sec}}}{p_i^{\mathrm{prim}}} \geq b \\ 1 & \frac{p_i^{\mathrm{sec}}}{p_i^{\mathrm{prim}}} < b \end{cases} \tag{7}$$

and the critical pressure ration b. For a more compact notation we introduce the vector

$$\boldsymbol{p} := \Big[\underbrace{p_1\ p_2}_{\downarrow \tau_1}\ \underbrace{p_3\ p_4\ p_5\ p_6}_{\downarrow \tau_2}\ \underbrace{p_7\ p_8}_{\downarrow \tau_3} \Big]^T \tag{8}$$

incorporating the eight pressures of the eight pneumatic muscles.

2.2 Mechanical Model

The robot represents a mechanical multibody system as sketched in Figure 2. We model the sections as cylinders with an evenly distributed mass and furthermore take a mass at the tool-center-point into account. The mechanical model is derived using Lagrange's equations of the second kind leading to a compact representation of the mechanical model. Introducing the vector of generalized coordinates

$$\boldsymbol{q} = [\,\alpha_1\ \alpha_2\ \alpha_3\,]^T \tag{9}$$

and assuming only conservative generalized forces act on the system – except the driving torques – the Lagrange formalism yields the mechanical equations of motion

$$\boldsymbol{M}(\boldsymbol{q})\ddot{\boldsymbol{q}} + \boldsymbol{c}(\boldsymbol{q}, \dot{\boldsymbol{q}}) + \boldsymbol{g}(\boldsymbol{q}) = \boldsymbol{\tau}(\boldsymbol{q}, \boldsymbol{p}). \tag{10}$$

In (10), $\boldsymbol{M}(\boldsymbol{q})$ describes the positive definite mass-matrix, $\boldsymbol{c}(\boldsymbol{q}, \dot{\boldsymbol{q}})$ the Coriolis momenta, $\boldsymbol{g}(\boldsymbol{q})$ the weight momenta, and $\boldsymbol{\tau}(\boldsymbol{q}, \boldsymbol{p})$ the driving torque. At this point, note that

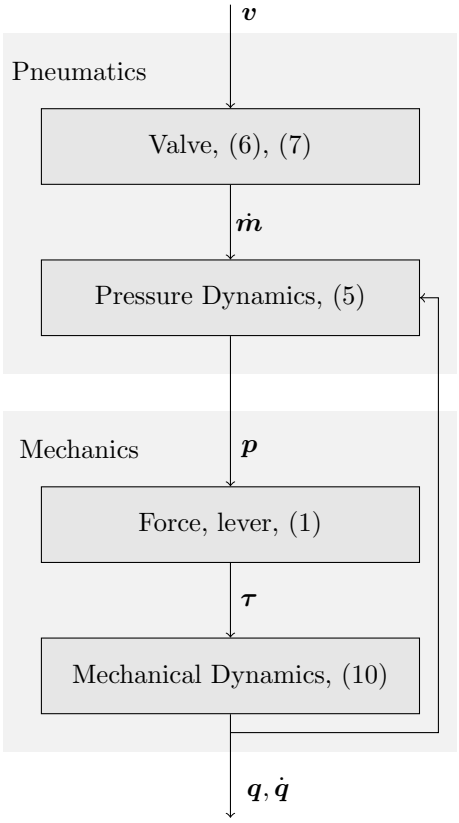

Fig. 3. Scheme of the overall model structure containing the pneumatic and mechanical subsystems.

the driving torque $\boldsymbol{\tau}(\boldsymbol{q}, \boldsymbol{p})$ also depends on the pressures $\boldsymbol{p}$, as they are a result of the muscle forces and their corresponding lever. The forces depend on the pressures as well as on the lengths of the muscles, which in turn are depending on the angles $\boldsymbol{q}$.

As the actuation of each joint is based on the antagonist principle, the driving torque at each joint l is a superposition of the forces F_l^{pos} (resulting in a positive momentum) and F_l^{neg} (resulting in a negative momentum) multiplied by the lever d_l:

$$\tau_l = d_l(F_l^{\mathrm{pos}} - F_l^{\mathrm{neg}}). \tag{11}$$

Later in Section 3, when introducing the control, we will express the forces by their mean value F_l^{mean} and difference ΔF_l as

$$F_l^{\mathrm{pos}} = F_l^{\mathrm{mean}} + \Delta F_l \tag{12}$$
$$F_l^{\mathrm{neg}} = F_l^{\mathrm{mean}} - \Delta F_l. \tag{13}$$

Then, the driving torque becomes

$$\tau_l = d_l \Delta F_l \tag{14}$$

and the mean Force F_l^{mean} is a degree of freedom utilized for determining the stiffness of the controlled joint.

2.3 Overall System

Combining the pneumatic model (5), (6), (7) and the mechanical model (10), we arrive at the overall system description illustrated in Figure 3. The pneumatic part of the system is divided into the valve function and the pressure dynamics. The valve function is modeled as a

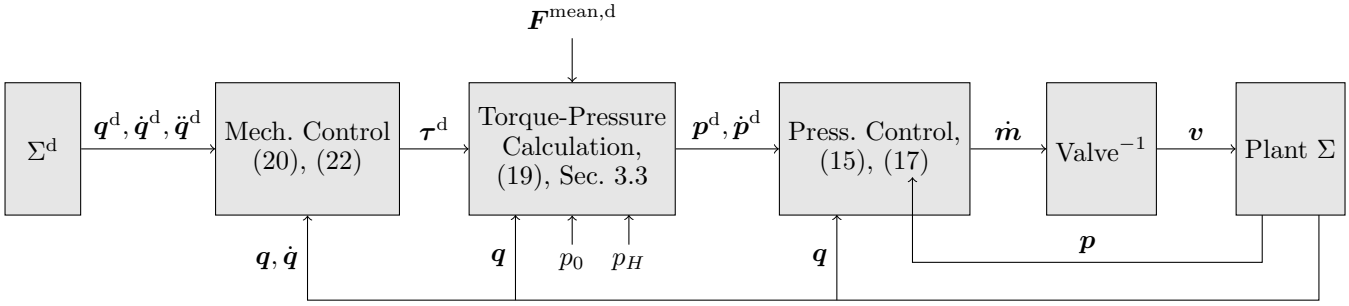

Fig. 4. Closed-Loop System resulting from the design process in Section 3. The inner control loop regulates the pressure – and therefore torques – while the outer mechanical control loop ensures the trajectory tracking for $\boldsymbol{q}$.

static relation from control input v to mass flow $\dot{m}$ and will later be inverted. Therefore, we will use the mass flow $\dot{m}$ as the input to our system for control design purposes. It can also be seen that the pneumatic and mechanical part of the system are not decoupled since the volumes and their derivatives play an important role for the pressure dynamics.

3. CONTROL DESIGN

To achieve the goal of trajectory tracking for a given trajectory of the angles $\boldsymbol{q}$, we employ a cascaded control structure: underlying the mechanical control loop, a pressure controller is implemented. We first describe this pressure controller in the following section before presenting the mechanical feedback control.

3.1 Pneumatic Control

The pneumatic part of the system consists of eight decoupled nonlinear differential equations of the form (5). As mentioned before, the valve function (6) is inverted and we therefore assume to have the mass flows $\dot{m}_i$ as control inputs.

By choice of

$$\dot{m}_i = \frac{1}{R_s T}\left(\frac{V_i(s_i)}{\kappa}\nu_i^{\text{pneu}} + p_i \dot{V}_i(s_i, \dot{s}_i)\right) \tag{15}$$

we achieve an exact input-to-state linearization with the newly introduced, virtual input ν_i^{pneu} by plugging in the mass flow to the pneumatic system (5):

$$\dot{p}_i = \nu_i^{\text{pneu}}. \tag{16}$$

Following this exact linearization we apply the feedback control

$$\nu_i^{\text{pneu}} = \dot{p}_i^{\text{d}} + K_i(p_i^{\text{d}} - p_i) \tag{17}$$

with the desired pressure p_i^{d}, its time derivative $\dot{p}_i^{\text{d}}$, and the control gains $K_i > 0$. By this the pressure dynamics (5) result in the asymptotically stable closed loop dynamics

$$(\dot{p}_i - \dot{p}_i^{\text{d}}) + K_i(p_i - p_i^{\text{d}}) = 0. \tag{18}$$

3.2 Mechanic Control

The input to the mechanical system is given by the pressures $\boldsymbol{p}$. Our following mechanical control law will use the three torques at the rotary joints as control input. Hence, a computation of the desired pressures

$$\boldsymbol{p} = f(\boldsymbol{q}, \boldsymbol{\tau}^{\text{d}}) \tag{19}$$

depending on the desired torque $\boldsymbol{\tau}^{\text{d}}$ has to be applied. This relation is given by the force function of the muscles (1), combined with the force-torque relation (11). The pressure-torque-relation (19) is a static relation bringing the mean force for each muscle pair as a degree of freedom. The assignment of those mean forces is described in Section 3.3.

The outer mechanic control loop is designed using a computed-torque ansatz. Applying the torque

$$\boldsymbol{\tau} = \boldsymbol{M}(\boldsymbol{q}^{\text{d}})\boldsymbol{\nu}^{\text{mech}} + \boldsymbol{c}(\boldsymbol{q}^{\text{d}}, \dot{\boldsymbol{q}}^{\text{d}}) + \boldsymbol{g}(\boldsymbol{q}^{\text{d}}) \tag{20}$$

to the mechanical system (10) yields the exact input-to-state linearized, decoupled system

$$\ddot{\boldsymbol{q}} = \boldsymbol{\nu}^{\text{mech}} \tag{21}$$

for the newly introduces virtual input $\boldsymbol{\nu}^{\text{mech}}$. The system described by (21) consists of three double integrators, for which a PD-control law

$$\boldsymbol{\nu}^{\text{mech}} = \ddot{\boldsymbol{q}}^{\text{d}} + \boldsymbol{K}^{\text{P}}(\boldsymbol{q}^{\text{d}} - \boldsymbol{q}) + \boldsymbol{K}^{\text{D}}(\dot{\boldsymbol{q}}^{\text{d}} - \dot{\boldsymbol{q}}) \tag{22}$$

is a suitable choice. Here, $\boldsymbol{q}^{\text{d}}$ represents the desired trajectory of the angles with its corresponding time derivatives $\dot{\boldsymbol{q}}^{\text{d}}$, $\ddot{\boldsymbol{q}}^{\text{d}}$ and

$$\boldsymbol{K}^{\text{P}} = \text{diag}\Big(\begin{bmatrix} K_1^{\text{P}} & K_2^{\text{P}} & K_3^{\text{P}} \end{bmatrix}\Big) \tag{23}$$

$$\boldsymbol{K}^{\text{D}} = \text{diag}\Big(\begin{bmatrix} K_1^{\text{D}} & K_2^{\text{D}} & K_3^{\text{D}} \end{bmatrix}\Big) \tag{24}$$

are the control gains. The remaining closed-loop mechanical dynamics then become

$$\Big(\ddot{\boldsymbol{q}} - \ddot{\boldsymbol{q}}^{\text{d}}\Big) + \boldsymbol{K}^{\text{D}}\Big(\dot{\boldsymbol{q}}^{\text{d}} - \dot{\boldsymbol{q}}\Big) + \boldsymbol{K}^{\text{P}}\Big(\boldsymbol{q}^{\text{d}} - \boldsymbol{q}\Big) = 0 \tag{25}$$

which is an asymptotically stable system for a proper choice of the control gains $\boldsymbol{K}^{\text{P}}$ and $\boldsymbol{K}^{\text{D}}$ with $\boldsymbol{K}^{\text{P}}, \boldsymbol{K}^{\text{D}} \succ 0$.

3.3 Stiffness of the System

The mean force of each of the joints represents its stiffness: a low mean force results in a soft behavior, while a large mean force at a joint corresponds to a very stiff system. However, the single muscle forces F_i are bounded

- from below since pneumatic muscles can only produce traction forces, i.e. $F_i \geq 0$, and
- from above since there is a maximal force $F_i^{\max}(\boldsymbol{q}, p_H)$ achieved at supply pressure p_H and depending on the joint configuration.

Thus, the robot cannot realize every stiffness in any configuration $\boldsymbol{q}$. To optimally exploit the range of possible mean forces, we propose the following procedure, explained

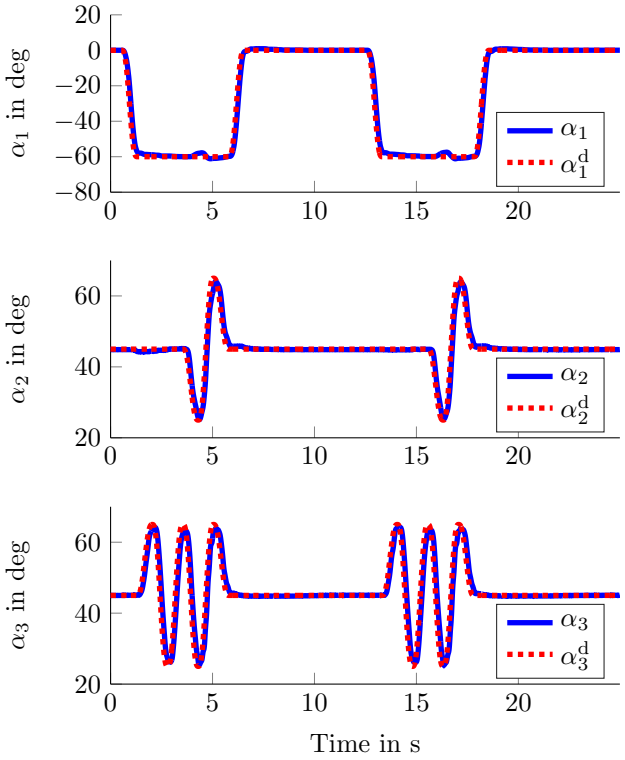

Fig. 5. Time plot of the angles of the feedback controlled robot with a desired sample trajectory (red, dotted).

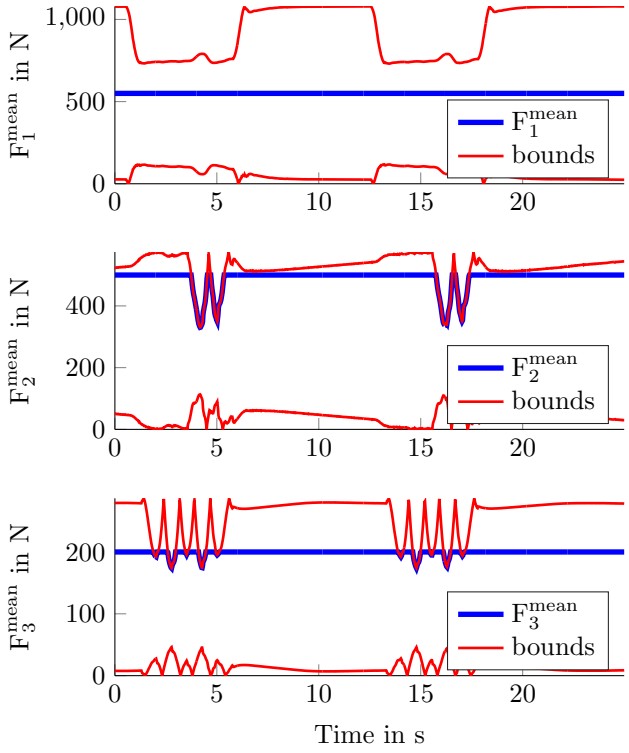

Fig. 6. Mean Forces with their boundaries for the angle trajectories in Figure 5. In situations where the desired mean force cannot be realized, it is adapted to the boundaries.

for a single joint l. After a desired mean force $F_l^{\mathrm{mean,d}}$ and a demanded difference force $\Delta F_l = \tau_l / d_l$ for a joint is given do the following:

(1) Compute the maximal force $F_l^{\max}(\boldsymbol{q}, p_H)$ and the minimal force $F_l^{\min}(\boldsymbol{q}, p_{\min}) \geq 0$ of the antagonists of joint l.
(2) Determine the minimal and maximal mean force $F_l^{\mathrm{mean,min}}$ and $F_l^{\mathrm{mean,max}}$, which are given by constraining the demanded difference force ΔF_l on the interval of possible forces $[F_l^{\min}, F_l^{\max}]$. If the demanded difference force cannot be achieved in the current configuration $\boldsymbol{q}$, i.e. $|\Delta F_l| > \left|F_l^{\max} - F_l^{\min}\right|$, we choose the mean value of $F_l^{\min}$ and $F_l^{\max}$ as the mean force F_l^{mean}.
(3) If $|\Delta F_l| \leq \left|F_l^{\max} - F_l^{\min}\right|$, set the mean force as the constrained desired mean force $F_l^{\mathrm{mean}} = \max(\min(F_l^{\mathrm{mean,d}}, F_l^{\mathrm{mean,max}}), F_l^{\mathrm{mean,min}})$.

3.4 Practical Realization of the Control Scheme

For the practical realization of the control law, the pressures $\boldsymbol{p}$, angles $\boldsymbol{q}$, and their time-derivatives $\dot{\boldsymbol{q}}$ have to be known. They either have to be measured and filtered or reconstructed using an observer. To improve the robustness of the closed-loop system, we use the desired values $\boldsymbol{q}^{\mathrm{d}}$, $\dot{\boldsymbol{q}}^{\mathrm{d}}$ to exactly linearize the mechanical equations in (20) and hence implement a feed-forward linearization of the mechanical system. Furthermore, we made simplifications during the modeling process in Section 2. In order to eliminate steady-state errors of the closed-loop system, mainly caused by model errors, an anti-wind-up integrator term can be added to the mechanical control law (22).

Preceding the feed-back control laws of the pneumatic and mechanical system, the trajectories $\boldsymbol{p}^{\mathrm{d}}(t)$, $\dot{\boldsymbol{p}}^{\mathrm{d}}(t)$, $\boldsymbol{q}^{\mathrm{d}}(t)$, $\dot{\boldsymbol{q}}^{\mathrm{d}}(t)$, and $\ddot{\boldsymbol{q}}^{\mathrm{d}}(t)$ have to be calculated. We provide the trajectories $\boldsymbol{q}^{\mathrm{d}}(t)$, $\dot{\boldsymbol{q}}^{\mathrm{d}}(t)$, $\ddot{\boldsymbol{q}}^{\mathrm{d}}(t)$ as polynomial functions, and the desired mean forces $F_l^{\mathrm{mean,d}}$ to the controller. Online, the controller then computes the pressure trajectories $\boldsymbol{p}^{\mathrm{d}}(t)$ and their time derivatives $\dot{\boldsymbol{p}}^{\mathrm{d}}(t)$.

3.5 Overall Control Scheme

The here presented control scheme is depicted in Figure 4. The derivative of the desired pressures $\dot{\boldsymbol{p}}^{\mathrm{d}}$ used as the feed-forward signal for the pressure dynamics is obtained via differentiation. Due to this differentiation or high-pass filtering, a sufficiently smooth input trajectory for the angles $\boldsymbol{q}^{\mathrm{d}}(t)$ has to be provided in order to increase the performance of the system.

4. EXPERIMENTAL RESULTS

The control law introduced in the previous section has now been applied to the real system. Figure 5 shows the time behavior of the angles for a desired trajectory with variations in all three joints. The (red dotted) desired trajectory is tracked well by the measured angles, even for the quite large variations in the desired angles and situations with coupled motions.

Figure 6 illustrates the corresponding time plot of the mean forces F_l^{mean} with their boundaries $F_l^{\mathrm{mean,min}}$ and $F_l^{\mathrm{mean,max}}$ according to the procedure described in Section 3.3. In the shown case, the system cannot realized the (constant) desired mean force of the three joints in every

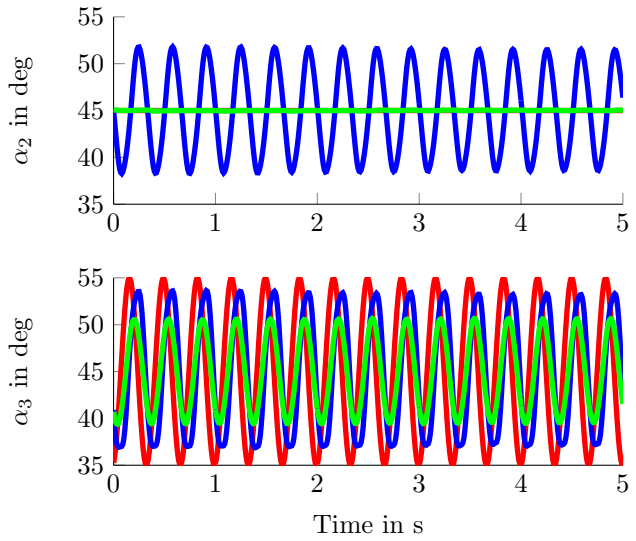

Fig. 7. Effect of couplings in α_2 and α_3. An excitation of α_3 (red: desired) results in an oscillation of α_2 if the couplings are neglected in the control law (blue). Taking the couplings into account keeps α_2 at its desired constant value (green).

situation. Therefore, the mean force is adapted to ensure a proper trajectory tracking of the closed-loop system. The major influences on the realizable mean force are

- structural limitations – i.e. the pneumatic muscles have a maximal force depending on their length,
- dynamical aspects – e.g. if a motion requires a large torque, hence a large difference of forces of the antagonists, but the muscle forces are constraint to a certain interval, and
- limitations du to weight compensation – i.e. to compensate the gravitational forces, a certain torque has to be applied. Depending on the desired mean force and the actual configuration $\boldsymbol{q}$, this weight compensation can limit the range of realizable mean forces.

Completing, Figure 7 illustrates the effect of dynamical couplings between the α_2 and α_3 of the robot. Having the same rotational axis, they influence each other. In the given plot, α_3 is excited with a sinusoidal signal of 3Hz, while α_2 should be a constant angle (desired trajectories printed in red color). The blue line illustrates the behavior without the decoupling effects of the computed torque controller (20), i.e. using only the diagonal elements of the mass-matrix $\boldsymbol{M}(\boldsymbol{q})$. The green trajectory corresponds to the fully applied control law. In the illustrated case, neglecting the couplings in the feedback control law results in an undesired excitation of α_2 with an amplitude of about 5 degrees. At this point, note that the seemingly better tracking behavior of the blue line in α_3 is only a better amplitude response and arises from the resonance of α_2.

5. CONCLUSIONS

We have presented a model-based cascaded control concept for a robotic arm with three rotational degrees of freedom. The robot's actuation is based on antagonistically arranged pneumatic muscles. We regulate the pressure inside the muscles by feedback linearization and have given a mechanical control law for the robot. The stiffness of the overall system can then be set by the mean force of the antagonists. We further provided a strategy to adapt the mean force online in case it is required due to dynamical or other physical constraints. The designed control law was implemented to an experimental setup and shows a good closed-loop behavior and reveals the necessity of considering the mechanical couplings for the given system.

REFERENCES

Albu-Schäffer, A., Eiberger, O., Grebenstein, M., Haddadin, S., Ott, C., Wimböck, T., Wolf, S., and Hirzinger, G. (2008). Soft Robotics. *IEEE Robotics & Automation Magazine*.

Ament, C. and Eichhorn, M. (2010). Model-based Control Design of the Compliant Robot Arm "AirArm". In *IEEE International Conference on Control Applications*.

Bicchi, A. and Tonietti, G. (2004). Fast and "Soft-Arm" Tactics. *IEEE Robotics & Automation Magazine*.

Boaventura, T., Semini, C., Buchli, J., Frigerio, M., Focchi, M., and Caldwell, D.G. (2012). Dynamic Torque Control of a Hydraulic Quadruped Robot. In *IEEE International Conference on Robotics and Automation*.

Chou, C.P. and Hannaford, B. (1996). Measurement and Modelung of McKibben Pneumatic Artificial Muscles. *IEEE Trans. on Robotics and Automation*.

Falkenhahn, V., Hildebrandt, A., Neumann, R., and Sawodny, O. (2017). Dynamic Control of the Bionic Handling Assistant. *IEEE/ASME Transactions on Mechatronics*.

Ficuciello, F., Villani, L., and Siciliano, B. (2015). Variable Impedance Control of Redundant Manipulators for Intuitive Human-Robot Physical Interaction. *IEEE Trans. on Robotics*.

Grebenstein, M., Albu-Schäffer, A., Bahls, T., Chalon, M., Eiberger, O., Friedl, W., Gruber, R., Haddadin, S., Hagn, U., Haslinger, R., Höppner, H., Jörg, S., Nickl, M., Nothhelfer, A., Petit, F., Reill, J., Seitz, N., Wimböck, T., Wolf, S., Wüsthoff, T., and Hirzinger, G. (2011). The DLR Hand Arm System. In *IEEE International Conference on Robotics and Automation*.

Hildebrandt, A., Sawodny, O., Neumann, R., and Hartmann, A. (2003). A Cascaded Tracking Control Concept for Pneumatic Muscle Actuators. In *European Control Conference*.

Hildebrandt, A., Sawodny, O., Neumann, R., and Hartmann, A. (2005). Cascaded Control Concept of a Robot with two Degrees of Freedom Driven by four Artificial Pneumatic Muscle Actuators. In *American Control Conference*.

Jafari, A., Tsagarakis, N.G., Sardellitti, I., and Caldwell, D.G. (2014). A New Actuator With Adjustable Stiffness Based on a Variable Ratio Lever Mechanism. *IEEE/ASME Transactions on Mechatronics*.

Kronander, K. and Billard, A. (2016). Stability Considerations for Variable Impedance Control. *IEEE Trans. on Robotics*.

Laffranchi, M., Tsagarakis, N.G., and Caldwell, D.G. (2013). Analysis and Development of a Semiactive Damper for Compliant Actuation Systems. *IEEE/ASME Transactions on Mechatronics*.

Taghia, J., Wilkening, A., and Ivlev, O. (2012). Position Control of Soft-Robots with Rotary-Type Pneumatic Actuators. In *Proceedings of ROBOTIK 2012*.

Vanderborght, B., Albu-Schaeffer, A., Bicchi, A., Burdet, E., Caldwell, D., Carloni, R., Catalano, M., Eiberger, O., Friedl, W., Ganeshd, G., Garabini, M., Grebenstein, M., Grioli, G., Haddadin, S., Hoppner, H., Jafari, A., Laffranchi, M., Lefeber, D., Petit, F., Stramigioli, S., Tsagarakis, N., Damme, M.V., Ham, R.V., Visser, L., and Wolfa, S. (2013). Variable impedance actuators: A review. *Robotics and Autonomous Systems*.

Verl, A., Albu-Schäffer, A., Brock, O., and Raatz, A. (eds.) (2015). *Soft Robotics*. Springer.

Wang, X., Li, M., Guo, W., Wang, P., and Sun, L. (2013). Development of an antagonistic bionic joint controller for a musculoskeletal quadruped. In *IEEE/RSJ International Conference on Intelligent Robots and Systems*, 4466–4471.